# A Novel Loop Gain Adaptation Method for Digital CDRs Based on the Cross-Correlation Function

Javier Ardila and Elkim Roa
Integrated Systems Research Group - OnChip, Universidad Industrial de Santander
Bucaramanga, Colombia. E-mail: javier.ardila@correo.uis.edu.co, efroa@uis.edu.co

***Abstract*—Loop gain adaptation techniques that explore the dynamics of digital phase-locked loops, and clock and data recovery circuits through the autocorrelation function are becoming popular. This work proposes an adaptation technique based on the cross-correlation function between bang-bang phase detector and loop filter outputs instead. Filtering properties of the cross-power spectral density enhance the observability of loop dynamics allowing adaptation while maintaining the phase margin at a safe value. Compared to previously reported methods, the proposed adaptation technique directly tracks the CDR dynamics distinctively enhancing the gain adaptation algorithm.**

## I. Introduction

The loop dynamics of a bang-bang-based clock and data recovery circuit (BB-CDR) is affected by jitter noise sources in a receiver system [1]. Data input jitter or phase noise from the phase-locked loop (PLL) might change the dynamics of the CDR by modulating the bang-bang phase detector (BBPD) gain ($K_{BB}$). Although BB-CDR is a widely used recovery scheme considering its performance and digital-synthesized implementation [2], its loop dynamics suffer when high-frequency jitter constrains the loop gain. To overcome this phenomenon, a control mechanism to provide a constant loop gain is required to perform proper tracking and jitter suppression, such that a low bit error rate (BER) is maintained.

Several strategies that arise from digital PLLs (DPLL) solutions can be used to monitor the CDR dynamics by exploiting the autocorrelation function of the BBPD output [1], [3], [4]. Albeit these approaches seem to optimize the loop gain of the CDR, they are based on *a priori* assumptions regarding jitter sources or loop latency and do not guarantee a proper phase margin (PM) in the resulting adapted loop.

Recent works [5], [6] avoid *a priori* assumptions and guarantee a safe PM implementing adaptive gain based on data measurements. To efficiently accomplish this, they improve the observability of the autocorrelation function by adding a low-pass filter (LPF) at the BBPD output as Fig. 1 depicts. However, filtering the BBPD output demands a careful selection of the filter bandwidth (BW), which must be considered *a priori*. Regarding portability, the filter BW must be adjusted according to the specifications of different CDR designs. Besides, by applying the proposed approach in this paper, the extra hardware added by the LPF can be saved.

In [6] autocorrelation on the BBPD output is applied. In contrast, we propose the cross-correlation-based adaptive loop gain technique (XCALG), using two strategic points in the system by exploiting the filter properties of cross-power spectral

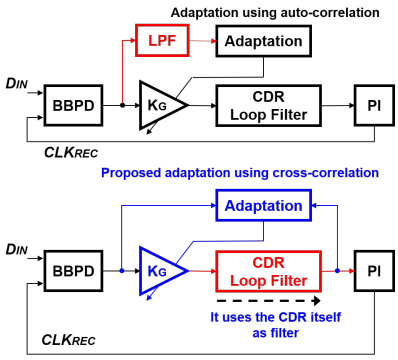


Fig. 1. Conventional and proposed adaptation concepts.

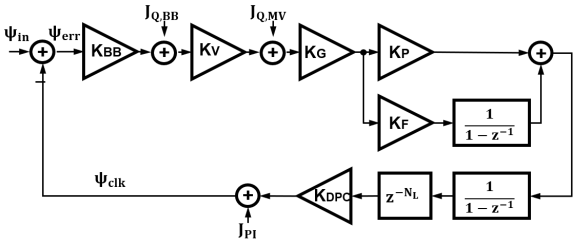


Fig. 2. Linear model of a DPLL-based CDR.

density (CPSD). We demonstrate how the CDR itself can be used as the required filter and how this filtering characteristic links to the CPSD without incurring in an extra LPF. Since the proposed method considerably enhances the CDR dynamics tracking, and improves the loop adaptation algorithm, we envision that XCALG could become the preferred method for gain adaptation.

## II. Spectral Analysis of Cross-Correlation

A conventional linear model for a DPLL-based CDR is shown in Fig. 2 [5]. Where $K_{BB}$ is the BBPD gain, $K_V$ the decimation gain via majority voting (MJV), $K_P$ and $K_F$ are the proportional and integral path gains, $K_{DPC}$ the digital to phase converter (DPC) gain, and $N_L$ the total equivalent delay around the loop. The jitter sources for this model are $\psi_{in}$ for input data jitter, $J_{Q,BB}$ and $J_{Q,MV}$ for quantization noise due to BBPD and MJV blocks respectively, and $J_{PI}$ representing the total jitter contribution coming from the phase interpolator (PI). $J_{PI}$ includes the quantization noise from PI and the noise from PLL. The loop gain transfer function is given by:

978-1-7281-0397-6/19/$31.00 ©2019 IEEE

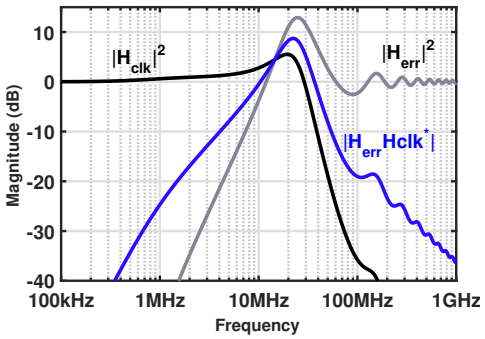


Fig. 3. Magnitude of $H_{err}(f)H_{clk}(f)^*$ and the power spectrum of $H_{clk}(f)$ and $H_{err}(f)$.

$$G(z) = K_{BB}K_V\left(K_P + \frac{K_F}{1-z^{-1}}\right)\frac{K_{DPC}}{1-z^{-1}}z^{-N_L}, \quad (1)$$

The input-output and input-error for jitter are given by,

$$H_{clk}(z) = \frac{G(z)}{1+G(z)}, \quad (2) \qquad H_{err}(z) = \frac{1}{1+G(z)}. \quad (3)$$

The power spectral density (PSD) for $\psi_{err}$ is given by,

$$S_{err}(f) = |H_{err}(f)|^2\left[S_{in}(f) + S_{PI}(f)\right] + |H_{clk}(f)|^2\left[\frac{S_{Q,BB}(f)}{K_{BB}^2} + \frac{S_{Q,MV}(f)}{(K_{BB}K_V)^2}\right], \quad (4)$$

and the cross-power spectral density (CPSD) associated to $\psi_{err}$ and $\psi_{clk}$ can be derived as,

$$S_{err,clk}(f) = |H_{err}(f)H_{clk}^*(f)|\left[S_{in}(f) + S_{PI}(f)\right] - |H_{clk}|^2\left[\frac{S_{Q,BB}(f)}{K_{BB}} + \frac{S_{Q,MV}(f)}{K_{BB}K_V}\right]. \quad (5)$$

The above Eqs. (4) and (5) indicate that the different transfer functions of the system shape the PSD of the jitter sources. Fig. 3 shows an example of the power of $H_{clk}(f)$ and $H_{err}(f)$, and the filter function $|H_{err}(f)H_{clk}(f)^*|$. The example illustrates a condition with a phase margin (PM) about 45°where peaking can be detected. The peaking is observed in $|H_{err}(f)|^2$ and allows detecting oscillations presented in the CDR due to poor PM. However, as Eq. 4 states, high frequency components coming from $\psi_{in}$ and $J_{PI}$ sources can appear in the autocorrelation because of the high-pass response of $|H_{err}(f)|^2$.

In contrast, using $S_{err,clk}(f)$ (Eq. (5)), $|H_{err}(f)H_{clk}(f)^*|$ filters high-frequency components for $\psi_{in}$ and $J_{PI}$ as shown in Fig. 3. The peaking is still presented and the oscillation due to system dynamics can be observed. In both cases, the $J_{Q,BB}$ and $J_{Q,MV}$ contributions are filtered trough $|H_{clk}(f)|^2$. The filtering property of the CPSD at in-band and out-band frequencies overcomes one of the flaws presented in the autocorrelation approach, which can be summarized as the dependence on the PSDs of the various jitter sources [5]. Consequently, we opted to investigate the cross-correlation function as a viable alternative to monitor the CDR dynamics achieving better suppression of the effects of jitter sources.

## III. Cross-Correlation and Proposed Technique

Two main factors are analyzed to evaluate cross-correlation as a monitoring function of the CDR dynamics: observability and the impact of the jitter profiles. We compare the autocorrelation on BBPD output $R_X(n)$, and cross-correlation of MJV and CDR loop filter outputs $R_{XY}(n)$. We read the phase state in the digital domain through the register at the input of PI instead at $\psi_{clk}$ considering practical convenience. Time-step simulations of the model in Fig. 2 are performed considering the inclusion of quantization noise from BBPD and MJV blocks which avoid to recalculate the gain for these blocks. The BBPD model is equivalent to a $sign(x)$ function in the time domain and a transition density (TD) mask is added after the BBPD in order to emulate the TD of random sequence bits. For simplicity, quantization noise regarding the PI can be ignored because random jitter sources are dominant concerning the lower bound in [5]. Therefore, the $J_{PI}$ represents the phase noise coming from PLL. If the contribution of quantization noise from PI cannot be ignored, then it can be included in $J_{PI}$ input and the same procedure can be executed.

### A. Observability Enhancement

To compare the observability between $R_X(n)$ and $R_{XY}(n)$, $J_{PI}$ contribution is set to 0 and Gaussian $\psi_{in}$ exercises the time-step model. A Gaussian $\psi_{in}$ with $\sigma = 0.04$UI (UI = Unit Interval) is injected into the system for two different conditions. First, $K_G$ is set to 2.5, resulting in a PM about 45°, and second, $K_G$ is set to 1 obtaining a PM greater than 60°. For both conditions, the normalized right-half bands of $R_X$ and $R_{XY}$ are shown in Fig. 4. Results show a clear advantage in $R_{XY}(n)$ observability with respect to the $R_X(n)$ approach. Filtering on $R_X(n)$ is presented in [5], [6] as a solution to improve the observability, however, with the use of $R_{XY}(n)$ the additional filter is not necessary considering the reuse of the CDR loop as filter. Note that oscillations in $R_{XY}(n)$ appears for PM less than 60°(Fig.4(a)). However, when PM is higher than 60°these oscillations in $R_{XY}(n)$ are reduced considerably.

### B. Jitter Noise Profiles

Three different noise profiles are included. All these noise profiles have Gaussian $\psi_{in}$ with $\sigma = 0.04$UI. Profile 1 has $J_{PI} = 0$, profile 2 presents a -20 dB/dec roll-off with a power of -100dBc/Hz at 100kHz for $J_{PI}$, and profile 3 has a band-limited jitter with a first order roll-off of -20 dB/dec, cut frequency of 100MHz and an in-band level of -120dBc/Hz.

Fig. 5(a) presents comparison results between $R_X(n)$ and $R_{XY}(n)$ for profiles 1 and 2. The functions are scaled only for observability purposes. As expected, this experiment shows similar results for both approaches regardless of the jitter profiles. Both approaches $R_X(n)$ and $R_{XY}(n)$ filters the dominant low-frequency content.

On the other hand, Fig. 5(b) is clear evidence of how the two methods differ when high-frequency band-limited jitter, coming from PLL, is injected into the system. The content

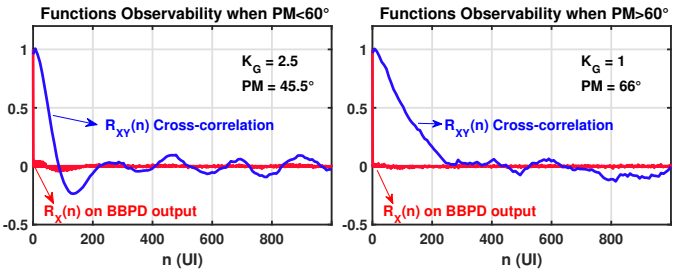


(a) (b)

Fig. 4. Observability comparison between $R_X(n)$ and $R_{XY}(n)$ for: a)$K_G$ set to 2.5, and b)$K_G$ set to 1.0.

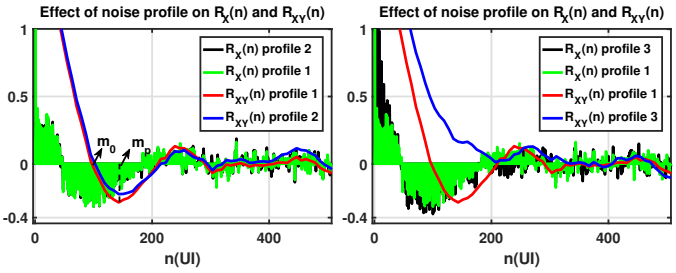


(a) (b)

Fig. 5. Correlation functions for different jitter profiles: (a) In-band, and (b) out-band $J_{PI}$.

of high frequencies coming from $J_{PI}$ adds the Gaussian $\psi_{in}$ leading to an average $K_{BB}$ gain reduction. This reduction leads a CDR less underdamped. The cross-correlation function filters the high-frequency content and reveals a system with less oscillation. In contrast, the autocorrelation function still presents oscillations, considering its high-pass shape, making difficult to extract information.

Although filtering the BBPD output reduces the oscillation on $R_X(n)$ as proposed in [5], there are still some system limitations with this approach in comparison with the use of $R_{XY}(n)$. First, careful selection of the filter bandwidth (BW) must be done manually. In contrast, $R_{XY}(n)$ performs this selection automatically due to the inherent filtering performed by the CDR itself and reflected in the CPSD. Second, to develop a very portable strategy, the filter BW must be adjusted according to the specifications of different CDR designs. Again, this is not a concern using the $R_{XY}(n)$ approach because the cross-correlation function selects the filtering BW directly from the CDR frequency response (Fig. 3).

### C. Proposed Loop Gain Adaptation

The results of the preceding analysis offer a compelling basis to explore and develop the XCALG. To do this, we consider the estimation of two key points in the $R_{XY}(n)$ function: $m_0$ and $m_p$. Both points are highlighted in Fig. 5(a). The $m_0$ value is that at which $R_{XY}(m_0) \approx 0$, and allows to estimate the first peak $R_{XY}(m_p)$. Forcing $R_{XY}(m_p)$ to be 0, an adaptation can be performed. We found a proper relation between them as,

$$m_p = \frac{3}{2} m_0. \tag{6}$$

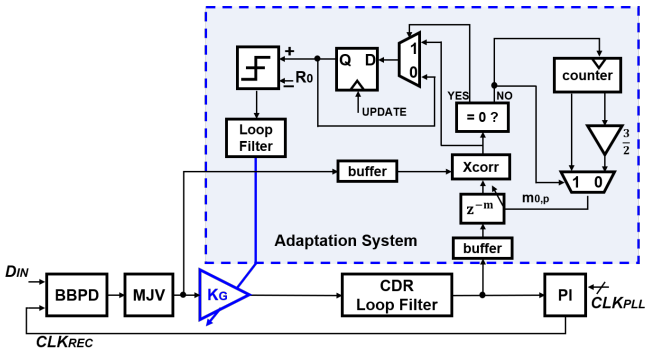


Fig. 6. Proposed XCALG implementation diagram.

The proposed XCALG diagram is depicted in Fig. 6. The XCALG takes the cross-correlation function between the MJV output and the CDR filter output and estimates a value that we call $R_{XY}(m)$ in two main phases. The first phase, consists in the estimation of $m_0$, the value at which $R_{XY}(m_0) \approx 0$. In the second phase, the adaptation calculates $m_p = \frac{3}{2} m_0$ obtaining an estimation of $R(m_p)$, then, compares this result with a threshold value $R_0$. Based on this comparison, $K_G$ increases or decreases and a new $R(m_0)$ estimation starts again. The adaptation process continues until a good PM is achieved. As studied in [5], total jitter $\psi_{err}$ starts to increase when the PM drops below 60°. We take advantage of this criteria by ensuring that CDR dynamics result in an adequate PM. Setting $R_0$ threshold to 0 gives a PM about 60°when the $K_G$ is adapted.

Unlike [5] and [6] that add a filter to clean autocorrelation results, we re-use the loop filter and apply cross-correlation to obtain a result independent of in-band and out-band jitter. Also, we reuse the adaptive delay block $z^{-m}$ which is set up with the proper delay depending on whether the adaptation is estimating $R(m_0)$ or $R(m_p)$.

## IV. Results and Discussion

Here we present simulations of a compliant USB3.0 CDR model as an example to validate the proposed XCALG. The CDR system parameters employed are: $K_P = 2$, $K_F = 2^{-6}$, $K_{DPC} = 2^{-10}$, $L = 8$, $TD = 0.5$ and $N_L = 5 * L = 40$ assuming 5 pipeline stages in the digital synthesis of the CDR loop filter. The jitter conditions are given as follows: Test 1) $\psi_{in}$ with $\sigma = 0.06$UI, test 2) $\psi_{in}$ with $\sigma = 0.04$UI, test 3) $\psi_{in}$ with $\sigma = 0.03$UI, test 4) $\psi_{in}$ with $\sigma = 0.04$UI and a phase noise in $J_{PI}$ described by a -20 dB/dec roll-off with a power of -90dBc/Hz at 100kHz, and test 5) $\psi_{in}$ with $\sigma = 0.04$UI and band-limited phase noise in $J_{PI}$ with a first order rolloff -20 dB/dec, cut frequency of 100MHz and in-band level of -115dBc/Hz. The XCALG uses a $M = 16380$ of buffer size. Although autocorrelation and cross-correlation operations demand large size buffers, system buffers can be allocated to reduce area penalty. $R_0$ is set to 0 to achieve PM about 60°, and the gain-step for each update $\Delta K_G$ is set to 0.05. The UPDATE signal refreshes $K_G$ for each $M$ observed sample.

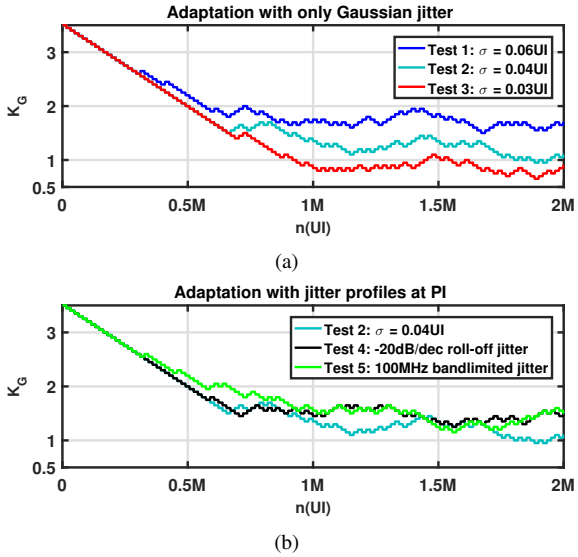


Fig. 7. Evolution of the adapted $K_G$ for (a) only Gaussian $\psi_{in}$, and (b) Gaussian $\psi_{in}$ and jitter profiles injected in $J_{PI}$.

Fig. 7 demonstrates that the XCALG converges to an adapted $K_G$ value for each case of jitter conditions. Fig. 7(a) shows the results for tests 1,2, and 3. As expected, a large amount of random noise decreases the CDR loop gain, thus the $K_G$ obtained from adaptation is proportional to $\sigma$. Fig. 7(b) shows the results for tests 3 and 4, where the jitter profiles are included in the $J_{PI}$ signal, and test 2 is repeated only for reference. The adaptation technique converges to similar $K_G$ values in both cases, as theoretical filter properties of the CPSD predicts. In comparison with the test 2, it is observed a slightly increment in the adapted $K_G$ which is due to the remaining jitter that still can be observed by the BBPD. For all cases, the dithering presented at the end of the adaptation can be reduced by adding hysteresis.

Adapted $K_G$ results in a CDR loop with optimized PM$\approx 60^\circ$ regarding jitter suppression and stability. With this, the jitter-tolerance (JTOL) curve does not present any ringing and therefore the eye aperture is maximized, leading a system with an improved BER. The result of the XCALG can also be studied, by using test 2 and test 3 setups, to explore the effectiveness of the adaptation by extracting the optimal $K_G$ which improves the high-frequency JTOL response. To do this, the $K_G$ value is manually swept and no adaptation is implemented. For each $K_G$, the minimum JTOL value is extracted using time-step simulations. Fig. 8(a) plots the results using continuous lines. Optimal values are obtained with $K_G$ between $1 - 1.5$ for $\sigma = 0.03$UI, and $0.9 - 1.2$ for $\sigma = 0.04$UI. The highlighted point in each curve corresponds to the $K_G$ value reached by our XCALG after dither suppression, demonstrating that the adapted $K_G$ is near to the optimal.

Fig. 8(b) clarifies how each minimum JTOL (Min JTOL) point in Fig. 8(a) is obtained using the test 3 as example. For low frequencies, the JTOL decreases with low $K_G$ degrading the tracking capability for low-frequency jitter as in a sinusoidal jitter (SJ) tolerance test. This is a well known trade-off between the high and low frequency response of JTOL. Although the work presented in [6] suggests an alternative to alleviate this issue, they do not establish details on how to implement it and nor discussion is presented on the adaptation criteria. We envision a possible approach as follows: take more samples in the $M$-size buffers in order to observe lower frequencies in the correlation functions, and keep monitoring the $R_{XY}(n)$ to capture oscillations due to SJ. However, trying to monitor low frequencies due to SJ exacerbates the complexity of the digital implementation and area penalty. For this reason, we consider that the trade-off between a well-damped system and the degradation of the JTOL at low frequencies is still an open discussion and an opportunity for future works.

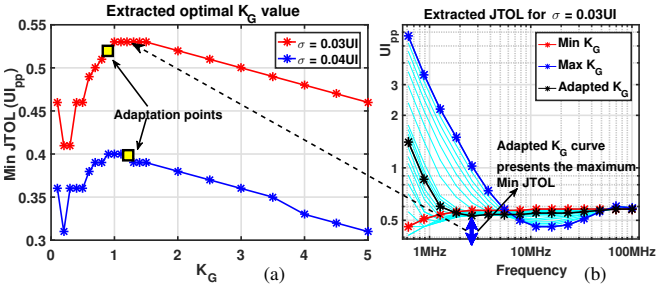


Fig. 8. Extracted optimal $K_G$, (a) via manual seeking and via adaptation technique. (b) Example of how each point of extracted $K_G$ is obtained from JTOL curve.

## V. Conclusion

In this paper, the cross-correlation-based adaptive loop gain technique (XCALG) is proposed. We devised the proposed technique exploiting the inherent link between the cross-correlation function and the CPSD. Following the performance results, the filtering properties of the CPSD decrease the impact of in-band and out-band jitter on the shape of the $R_{XY}(n)$ function as expected. The above observation reveal two important highlights: 1) function $R_{XY}(n)$ is a weak function of jitter noise; 2) Monitoring function $R_{XY}(n)$ emphasizes just on the CDR dynamics.

## References


[1] T. Kuan and S. Liu, "A Loop Gain Optimization Technique for Integer-$N$ TDC-Based Phase-Locked Loops," *IEEE Trans. Circuits Syst. I*, vol. 62, no. 7, pp. 1873–1882, July 2015.

[2] M. Talegaonkar, R. Inti, and P. K. Hanumolu, "Digital Clock and Data Recovery Circuit Design: Challenges and Tradeoffs," in *2011 IEEE Custom Integrated Circuits Conference (CICC)*, Sept 2011, pp. 1–8.

[3] S. Jang *et al.*, "An Optimum Loop Gain Tracking All-Digital PLL Using Autocorrelation of BangBang Phase-Frequency Detection," *IEEE Trans. Circuits Syst. II*, vol. 62, no. 9, pp. 836–840, Sept 2015.

[4] S. Kwon *et al.*, "An Automatic Loop Gain Control Algorithm for Bang-Bang CDRs," *IEEE Trans. Circuits Syst. I*, vol. 62, no. 12, pp. 2817–2828, Dec 2015.

[5] J. Liang *et al.*, "Loop Gain Adaptation for Optimum Jitter Tolerance in Digital CDRs," *IEEE J. Solid-State Circuits*, vol. 53, no. 9, pp. 2696–2708, Sept 2018.

[6] ——, "A 28Gb/s Digital CDR With Adaptive Loop Gain for Optimum Jitter Tolerance," in *2017 IEEE International Solid-State Circuits Conference (ISSCC)*, Feb 2017, pp. 122–123.